Available online at website: https://journal.bcrec.id/index.php/bcrec

Bulletin of Chemical Reaction Engineering & Catalysis, 20 (2) 2025, 221-233

Research Article

Sustainable Development of $ZnSO_4 \cdot H_2O$ and ZnO via Gelatin-Based Colloids for Advance Dye Photodegradation

Maria Ulfa*, Hilmia Aziza

Chemistry Education Study Program, Faculty of Teacher Training and Education, Sebelas Maret University, Jl. Ir. Sutami 36A, Surakarta 57126, Indonesia.

Received: 28th November 2024; Revised: 17th January 2025; Accepted: 6th February 2025
Available online: 10th February 2025; Published regularly: August 2025

Abstract

This study looks at how to sustainably develop $ZnSO_4 \cdot H_2O$ (Gunningite) and ZnO (Wurtzite) nanoparticles using gelatin-based colloids, focusing on their ability to break down dyes. Zinc acetate and zinc sulfate heptahydrate were used as starting materials, with gelatin helping to stabilize the process. After heating at 550 °C for 4 hours, the nanoparticles were analyzed for their surface area and composition. Gunningite had a higher surface area of 61.5 m^2/g, compared to Wurtzite's 11.4 m^2/g. Elemental analysis showed Gunningite contained 71% zinc, 21% oxygen, and 2% sulfur, while Wurtzite had 69% zinc and 31% oxygen. The photocatalytic activity was tested by degrading methylene blue under UV light. Gunningite had better results, achieving 87% degradation compared to Wurtzite's 72%. This was due to Gunningite's larger surface area and smaller particle size, making it more effective for treating dye wastewater. Future studies could explore larger-scale synthesis and industrial uses.

Keywords: Gunningite; wurtzite; photodegradation; methylene blue

How to Cite: Ulfa, M., Aziza, H. (2025). Sustainable Development of $ZnSO_4 \cdot H_2O$ and ZnO via Gelatin-Based Colloids for Advance Dye Photodegradation. *Bulletin of Chemical Reaction Engineering & Catalysis*, 20 (1), 221-233. (doi: 10.9767/bcrec.20260)

Permalink/DOI: https://doi.org/10.9767/bcrec.20260

1. Introduction

Gunningite ($ZnSO_4 \cdot H_2O$) and Wurtzite (ZnO) represent two distinct zinc-based minerals [1,2], each characterized by unique chemical compositions, crystal structures, and formation environments [3,4]. Gunningite, a hydrated zinc sulfate mineral [5], crystallizes in a monoclinic system with low symmetry and forms under low-temperature [6], oxidizing conditions as a secondary mineral in sulfide vapor alteration zones [6]. In contrast, Wurtzite, a high-temperature polymorph of ZnO, adopts a hexagonal crystal system and often coexists with sphalerite in hydrothermal and metamorphic environments [7]. The differences in their physical properties further reflect their contrasting natures: Gunningite is softer, less dense, and highly soluble in water, making it distinct from the more robust and thermally stable Wurtzite [8]. Moreover, Wurtzite's piezoelectric properties, derived from its hexagonal lattice, offer potential for functional applications. This comparative understanding of Gunningite and Wurtzite underscores the role of mineralogical diversity in tailoring materials for environmental and industrial uses [3,9].

Due to its sulfate composition, gunningite does not exhibit the same optical properties as wurtzite which exhibits semiconducting properties and is often studied for its potential in electronics and optoelectronics due to its wide band gap (~3.37 eV) and photoluminescence Zn

* Corresponding Author.
Email: ulfa.maria2015@gmail.com; ariaulfa@staff.uns.ac.id (M. Ulfa)

[10,11]. Primarily a mineralogical curiosity, gunningite does not have significant industrial applications. In other hand, due to its semiconducting properties, wurtzite is of great interest in materials science, particularly for optoelectronic applications, such as light-emitting diodes (LEDs) and solar cells [12]. In natural, Gunningite ($ZnSO_4 \cdot H_2O$) and Wurtzite (ZnO) form under different geological and environmental conditions, leading to their distinct crystal structures and chemical compositions [13]. Gunningite is a secondary mineral that typically forms in the oxidation zones of zinc-rich sulfide ore deposits, such as sphalerite (ZnO) [3,10]. Its formation involves the chemical weathering and alteration of primary sulfide minerals in the presence of water and oxygen, which leads to the conversion of sulfides into sulfate minerals. The key factors for gunningite formation include: Oxidizing Environment: Gunningite forms when sulfide minerals, such as sphalerite, are exposed to oxygen and water. The oxidation of ZnO (sphalerite) produces zinc ions (Zn^{2+}) and oxygen ions (O^{2-}) [14,15].

Gunningite contains water in its crystal structure, so it typically forms in areas where there is some moisture, either from groundwater or surface water. It generally forms at relatively low temperatures compared to other zinc-bearing minerals, such as zinc sulfides.In some cases, gunningite can form when zinc sulfate-rich solutions evaporate, leaving behind the hydrated sulfate mineral.Gunningite is often associated with other secondary minerals like goslarite ($ZnSO_4 \cdot 7H_2O$), which can transform into gunningite through dehydration. Wurtzite is a primary mineral that typically forms under high-temperature and hydrothermal conditions. It is a polymorph of zinc sulfide (ZnO) and can form through several geological processes. Key factors in the formation of wurtzite include: Wurtzite commonly forms in hydrothermal veins, where hot, zinc-rich fluids from deep within the Earth ascend and precipitate zinc sulfide in the wurtzite structure as they cool. Wurtzite is a high-temperature polymorph of ZnO, meaning it forms at higher temperatures compared to the more common sphalerite (the cubic form of ZnO). At temperatures above approximately 1,020 °C, wurtzite becomes the stable form of ZnO. Wurtzite can also form during the metamorphism of zinc ore bodies, where heat and pressure cause the recrystallization of sphalerite into the hexagonal wurtzite structure [16].

The laboratory-scale synthesis of Gunningite is rarely performed, while the synthesis of Wurtzite typically relies on limited synthetic materials and involves the use of toxic chemicals, alongside high energy and cost demands. The use of natural materials has emerged as a popular approach to reduce environmental pollution in material synthesis reactions. Previous studies have successfully synthesized Gunningite and Wurtzite using synthetic templates; however, no research has yet explored the synthesis of Gunningite and Wurtzite using gelatin as a template, nor compared their photocatalytic performance in methylene blue degradation. This study aims to compare the characteristics of Gunningite and Wurtzite synthesized with gelatin and evaluate their performance as photocatalysts in methylene blue degradation.

2. Materials and Method

2.1 Materials

The materials used in this research include 37% HCl (Sigma-Aldrich, Merck KGaA, Mr 36.5 g/mol), aquadest (Smart-Lab, Mr 18 g/mol), triblock copolymer pluronic P123 (Sigma-Aldrich, Merck KGaA, Mr 5750 g/mol), commercial gelatin (Gelita, Mr 90,000 g/mol), tetraethyl orthosilicate (TEOS, Sigma-Aldrich, Merck KGaA, Mr 208.33 g/mol), zinc acetate dihydrate $Zn(CH_3COO)_2.2H_2O$ (pro analysis, Merck Germany), 98% H_2SO_4 (pro analysis, Merck, Mr 98.08 g/mol), methylene blue (Sigma-Aldrich, Merck KGaA, Mr 319.85 g/mol), plastic wrap, label paper, and tissue.

2.2 Synthesis of Gunningite

First, 0.0346 grams of gelatin was dissolved in 30 mL of water and mixed with 3.39 grams of $ZnSO_4$ heptahydrate. The mixture was stirred for 24 hours, then placed in a hydrothermal reactor at 100 ºC for 24 hours. After the hydrothermal process, the product was filtered and dried in an oven at 100 ºC for approximately 5 hours. Finally, calcination was performed using a muffle furnace at 550 ºC for 4 hours to remove impurities.

2.3 Synthesis of Wurtzite

A total of 3.704 g of zinc acetate ($Zn(CH_3COO)_2 \cdot 2H_2O$) and 0.03 g of gelatin were dissolved in 30 mL of ethanol. After allowing the solution to settle completely, it was filtered using filter paper and a Buchner funnel. The residue was washed three times with 100 mL of distilled water until the pH became neutral. The precipitate was then dried in an oven at 120 ºC for 12 hours and subsequently calcined in a furnace at 550 ºC for 4 hours (Figure 1).

2.4 Methylene blue photocatalysis

A 500 mL methylene blue solution at 10 ppm was prepared, and 200 mL of the solution was transferred into an Erlenmeyer flask within a photocatalytic reactor. A total of 20 mg of photocatalyst was added, resulting in a 5 ppm methylene blue solution. The catalyst was allowed to adsorb in a sealed, dark environment for 30

minutes to achieve homogeneity and adsorption equilibrium. Subsequently, the solution was distributed into 13 dark vials, with one labeled as "Co" to indicate the initial concentration. Over 30 minutes, every 10 minutes, three vials that were not exposed to UV light were removed. The remaining nine vials were placed in a shaker inside the reactor, where the photocatalytic process was initiated by turning on a 20-watt Xenon UV lamp. Samples of 5 mL were collected at 10-minute intervals and sealed to prevent further reactions. The absorbance of each vial was measured using a UV-Vis spectrophotometer at 665 nm immediately after the process or within 24 hours to prevent deactivation.

2.5 Characterizations

The instruments used for sample analysis include X-Ray Diffraction (XRD, Pananalytical, Version PW 3050/60), Fourier Transform Infrared (FTIR) Spectrophotometer (Shimadzu 21, 0.5 cm^{-1} resolution), and Scanning Electron Microscopy with Energy Dispersive X-Ray (SEM-EDX), where images were captured using a JEOL JSM-700 microscope at an accelerating voltage of 15.0 kV. Additionally, sample testing was conducted using an Ultraviolet-Visible (UV-Vis) Spectrophotometer (Shimadzu UV-3600) at a wavelength of 665 nm.

3. Result and Discussion

Figure 2 illustrates the XRD patterns of ZnO samples synthesized via hydrothermal treatment in the presence of gelatin. The diffraction peaks observed at 2θ values of 31.74°, 34.37°, 36.17°, 47.45°, and 56.52° correspond to the (100), (002), (101), (102), and (110) planes of the wurtzite ZnO structure, in agreement with JCPDS file 36-1451. The XRD pattern of ZnO synthesized from zinc sulfate exhibited prominent diffraction peaks at 2θ = 18.86°, 26.41°, 27.12°, 29.46°, 35.86°, 41.34°, 43.05°, 46.23°, 50.47°, 53.95°, 54.90°, and 56.92°, corresponding to the formation of gunningite crystals. This phase represents a stable hydrated form of $ZnSO_4$, further confirming the crystalline nature of the synthesized material. The XRD profiles reveal sharp and distinct diffraction peaks, indicating the absence of detectable impurities. These results confirm that the samples exhibit a single-phase structure with high crystallinity. The average crystallite size of the ZnO materials was calculated using the Scherrer equation, which is widely used for determining crystallite size from XRD data. The estimated average crystallite sizes for ZnO wurtzite samples synthesized hydrothermally in gelatin-containing solutions were determined to be 88 nm and ZnO Gunningite were 23 nm.

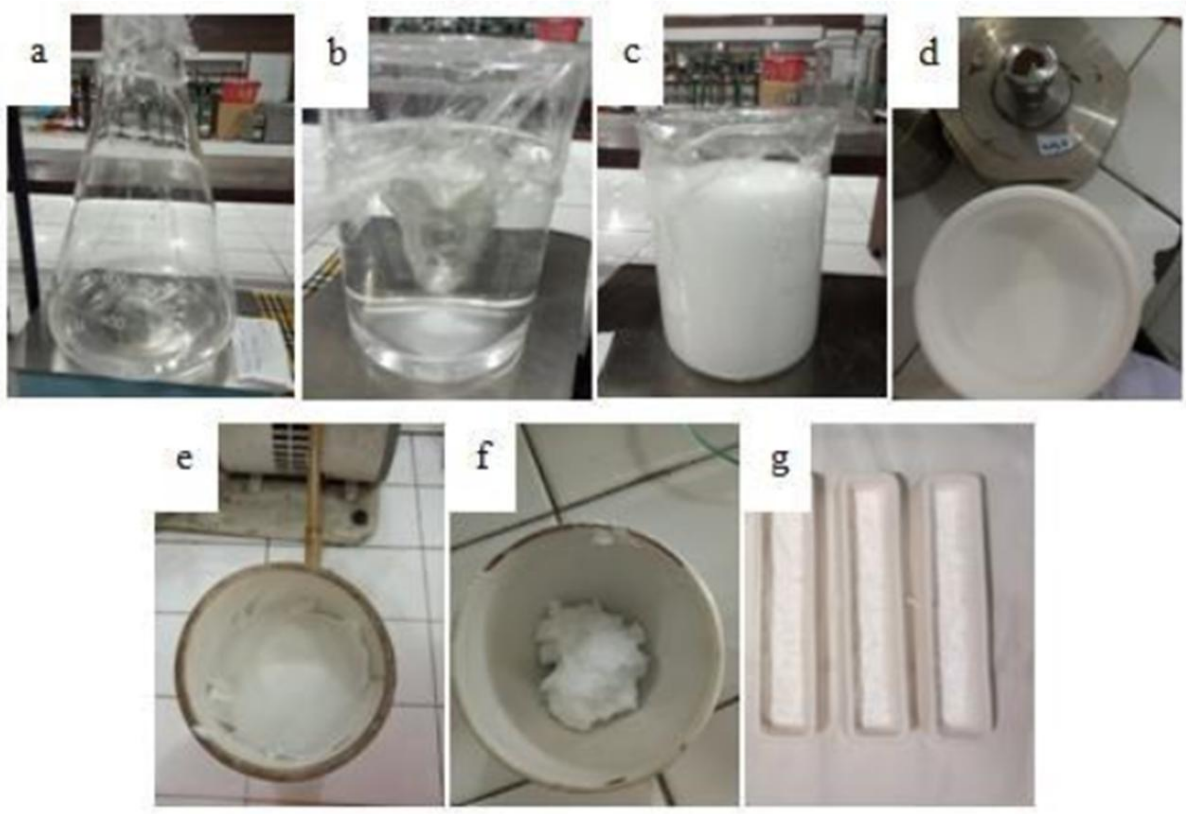

Figure 1. Synthesis Process: a) Dissolve zinc source ; b) Settle solution; c) Filter residue; d) Wash residue; e) Dry precipitate; f) Calcine sample; g) Pre-calcine h) Post-calcine

Figure 3 presents the FTIR spectra of ZnO synthesized via the hydrothermal method in gelatin-containing solutions. The FTIR spectra of the ZnO samples exhibit a broad absorption band in the 3200–3600 cm^{-1} range, corresponding to O–H stretching vibrations from adsorbed water molecules on the sample surface [17]. The intense FTIR absorption band at 443 cm^{-1} is assigned to Zn–O bond vibrations, further confirming the formation of the wurtzite ZnO structure [18]. No additional absorption bands were observed that would indicate the presence of carbon impurities within the structure. However, the powder sample derived from zinc sulfate (ZS) precursor exhibited a broad absorption band at 3420 cm^{-1}, which corresponds to the stretching vibrations of hydroxyl groups or adsorbed water molecules [19]. The band observed at 1671 cm^{-1} was attributed to the H-O-H bending vibration [20]. Furthermore, absorption bands at 1230 cm^{-1} and 1091 cm^{-1} were assigned to asymmetric and symmetric S=O stretching vibrations, respectively, providing clear evidence of the presence of sulfate anions within the structure [21]. The Zn-O bonds were characterized by a sharp peak at 505 cm^{-1}, while the low-intensity absorption peak at 419 cm^{-1} in the ZS sample was associated with the bending vibration of Zn-O in zinc hydroxide salt [22].

The SEM micrographs of ZnO in both Wurtzite and Gunningite phases reveal a densely packed cubic-like structure (Figure 4). It is postulated that the adsorption of gelatin onto the negatively charged O-terminated surface restricts growth along the c-axis, thereby promoting the development of the observed cubic morphology. When the zinc precursor was switched from zinc sulfate to zinc acetate, the densely aggregated cubic-like structures were observed to disaggregate into a more disordered arrangement.

The corresponding EDS spectrum for the Wurtzite phase confirmed the presence of only Zn and O, as evidenced by the characteristic X-ray peaks. The atomic composition was determined to be 51.32% Zn and 48.68% O. SEM analysis revealed that the particle sizes ranged from approximately 3.25 µm to 3.78 µm. In the case of Gunningite synthesized using zinc sulfate as a precursor, the SEM analysis demonstrated the formation of cubic particles with a size of approximately 3.25 µm. In contrast, Wurtzite synthesized from zinc acetate exhibited larger aggregates with a non-uniform morphology, with particle sizes measuring around 3.78 µm.

The effect of the zinc precursor on the photocatalytic performance of ZnO was thoroughly investigated via the photodegradation of methylene blue. ZnO in the Wurtzite phase, synthesized using zinc acetate with a gelatin template, exhibited a slightly lower methylene blue degradation efficiency compared to

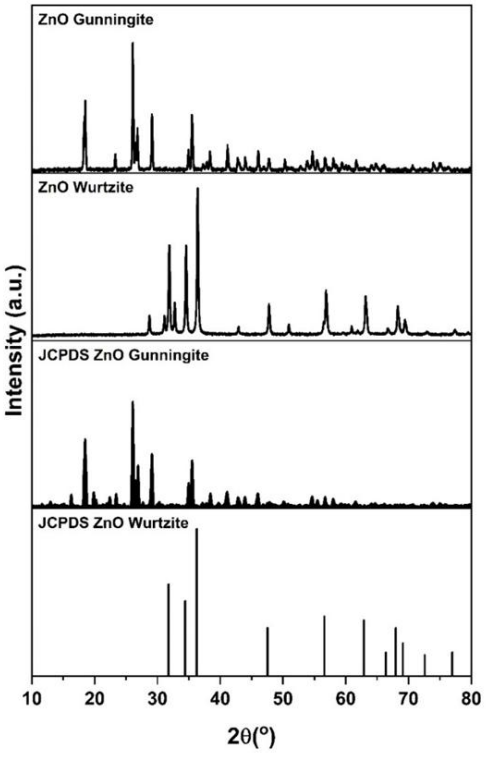

Figure 2. XRD of Gunningite and Wurtzite synthesis by gelatin and the standart

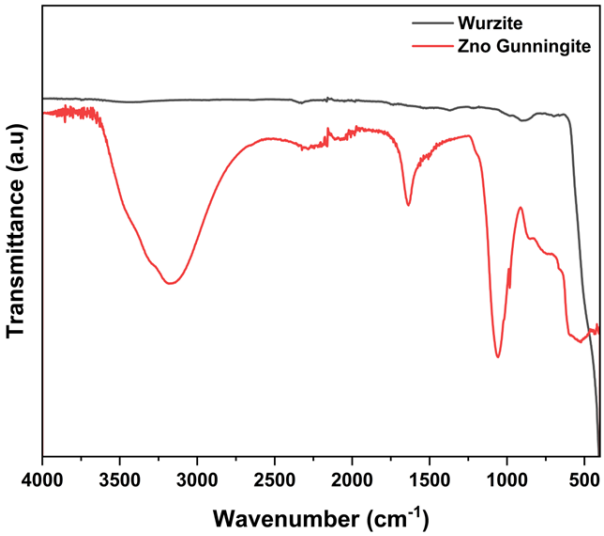

Figure 3. FTIR spectra of Wurtzite and Gunningite

Table 1. Crystallite size of Wurzie and Gunningite synthesis by presence of gelatin

Sample	Cristalinity (%)	Cristallyte size (nm)	Agregat size (µm)
ZnO Gunningite	53.47	23.80	3.25
ZnO Wurtzite	96.73	28.79	3.78

Gunningite, derived from zinc sulfate (Figures 5-6). The reduction in particle and crystallite sizes in Gunningite is postulated to increase the surface area and pore volume, thereby enhancing the adsorption of methylene blue molecules onto the catalyst surface during the photocatalytic process. Additionally, SEM and EDX analyses confirmed that Gunningite synthesized with gelatin as a template possesses uniform cubic-like structures containing sulfur atoms. The presence of sulfur is known to enhance the activity of chemisorbed oxygen species during aerobic photocatalytic reactions. These highly reactive oxygen species facilitate the formation of hydroxyl radicals, which are crucial for the photodegradation of methylene blue. In contrast (Figure 5), the Wurtzite phase synthesized with gelatin as a template, using zinc acetate as the precursor, did not incorporate sulfur as a functional group. As a result, the limited removal of MB was attributed to physical adsorption on the Zn and O surface. Photocatalytic experiments conducted under UV irradiation with an initial methylene blue concentration of 5 ppm achieved 87% and 72% removal efficiency within 90 minutes using Gunningite and Wurtzite, respectively, synthesized via the gelatin templating method (Figure 6).

The photocatalytic degradation mechanism begins with the excitation of electrons from the valence band to the conduction band of ZnO, creating hole (h^+):

$$ZnO + hv \rightarrow e^- + h^+ \quad (1)$$

Dissolved oxygen or O_2 adsorbed on the surface of the photocatalyst captures the excited electrons and is reduced to form superoxide radicals:

$$e^- + O_2 \rightarrow O_2^{\boxdot -} \quad (2)$$

The superoxide radicals then react with H_2O to produce hydroperoxide radicals ($HO_2\bullet$) and hydroxyl radicals ($OH\bullet$), both of which are strong oxidizing agents capable of degrading organic molecules:

$$O_2^{\boxdot -} + 2H_2O \rightarrow HO_2^{\boxdot} + OH^{\boxdot} \quad (3)$$

Simultaneously, the holes generated by light excitation are trapped by H_2O on the photocatalyst surface, leading to the formation of hydroxyl radicals ($OH^{\boxdot}$):

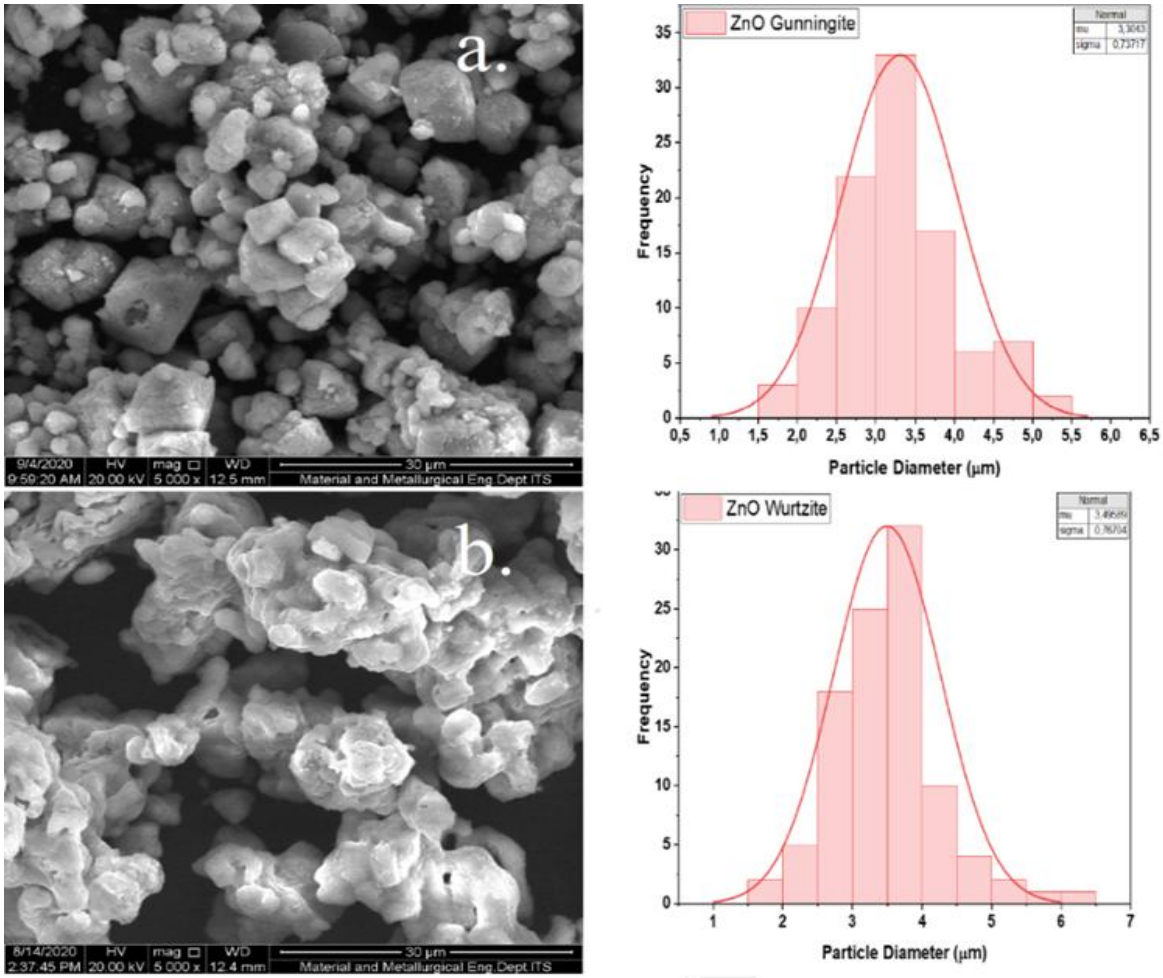

Figure 4. SEM and distribution particle of Gunningote and Wurtzite using gelatin as template

$$h^+ + H_2O \rightarrow OH^{\square} + H^+ \quad (4)$$

The hydroxyl radicals ($OH^{\bullet}$) then oxidize the organic pollutant (methylene blue) into carbon dioxide and water:

$$OH^{\bullet} + MB \rightarrow CO_2 + H_2O\ (degradation\ products) \quad (5)$$

Finally, recombination of the electron (e^-) and hole (h^+) occurs, completing the photocatalytic cycle:

$$e^- + h^+ \rightarrow ZnO \quad (6)$$

It can thus be concluded that the sample material with superior photocatalytic activity is Gunningite which syntesis by gelatin as template. This conclusion is supported by the characterization results of the Gunningie sample and its notable photocatalytic efficiency in degrading the methylene blue dye.

The adsorption-desorption isotherms of Gunningite ($ZnSO_4 \cdot H_2O$) and Wurtzite (ZnO) (Figure 8) nanoparticles were analyzed to better understand their surface properties and how these relate to their photocatalytic performance. The results revealed that Gunningite exhibited a significantly higher specific surface area (61.5 m²/g) compared to Wurtzite (11.4 m²/g), as seen in the adsorption isotherms. The higher surface area of Gunningite indicates a greater number of active sites available for adsorption, which is a crucial factor in the photocatalytic degradation of methylene blue. In contrast, Wurtzite's lower surface area limited its adsorption capacity, thus affecting its photocatalytic efficiency.

The adsorption-desorption behavior of both samples also correlates with their photocatalytic performance. Gunningite showed a much higher degree of methylene blue degradation (87%) under UV light, likely due to its larger surface area and smaller pore size (24.5 nm), which allow for more efficient adsorption and faster interaction with the substrate. On the other hand, Wurtzite, with a larger pore size (53.7 nm) and lower surface area, achieved a lower degradation rate (72%). This suggests that the surface properties, particularly the surface area and pore structure, play a crucial role in enhancing the photocatalytic activity of the materials. These findings underscore the importance of surface characteristics in determining the effectiveness of photocatalysts in environmental remediation applications.

Figure 5. Decolororisation of Methylene Blue after degraded by (a) Gunningite and (b) Wurtzite.

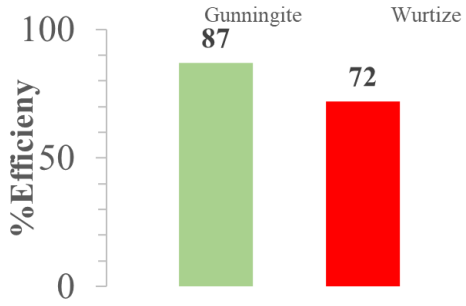

Figure 7. XRD of Gunningite and Wurtzite synthesis by gelatin and the standart from JCPDS ZnO of Gunningite and ZnO of Wurtzite

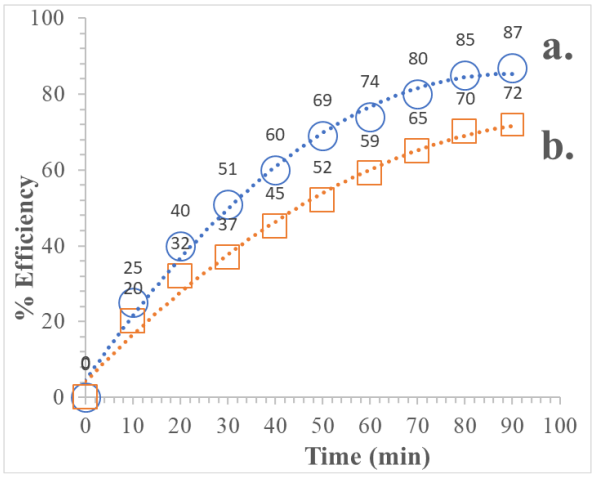

Figure 6. Methylene Blue Photodegradation of (a) Gunningite and (b)Wurtzite

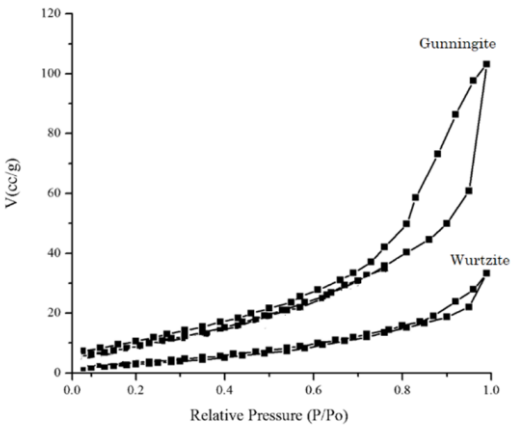

Figure 8. Isotherm adsorption-desorptio of Gunningite ($ZnSO_4 \cdot H_2O$) and Wurtzite (ZnO)

The adsorption performance in initial step of photodegradation of a material is closely related to its chemical composition, as revealed by elemental analysis using techniques such as Energy Dispersive X-ray (EDX). ZnO wurtzite, consisting of 69% zinc and 31% oxygen by weight, has a composition that supports its photocatalytic behavior, where zinc is the key component responsible for adsorbing methylene blue (Figure 9, Table 2). The high zinc content in ZnO provides sample active sites for the adsorption of methylene blue molecules, facilitating their interaction with the material during the photocatalysis process. However, its relatively lower oxygen content might limit the material's efficiency in some applications, as oxygen typically helps in improving the adsorption capacity and interaction with pollutants.

There are more active sites available for adsorption when materials like metal-organic frameworks (MOFs) or composites have a higher zinc concentration. Hydroxyl groups and other functional groups that aid in the binding of cationic dyes can be found in these active spots [23]. Methylene blue is a cationic dye, which means it is positively charged in solution. High Zn concentration might generate a positively charged environment on the adsorbent due to the presence of Zn^{2+} ions. This increases the electrostatic interaction between the positively charged MB molecules and the negatively charged sites on the adsorbent. Materials with high Zn content often exhibit greater surface area and porosity, which allows for more extensive contact between the adsorbent and dye molecules. A larger surface area provides more opportunities for adsorption to occur, thereby increasing overall capacity [24]. The inclusion of zinc can improve some chemical interactions between MB and the adsorbent. For example, Zn ions can interact with functional groups on the dye or adsorbent, enhancing adsorption efficiency [25]. The adsorption process is frequently pH-dependent. High Zn concentration may aid to maintain optimal pH conditions for dye adsorption. At specific pH values, the ionization of functional groups on the adsorbent may be adjusted to improve interaction with cationic dyes [24]. In contrast, gunningite, with a composition of 71% zinc, 21% oxygen, and 2% sulfur, demonstrates a more favorable adsorption profile. The higher zinc content compared to ZnO suggests that gunningite offers more available sites for adsorbing molecules. The presence of sulfur (2%) in gunningite, as indicated by the EDX analysis, introduces a chemical modification to the material that may alter the interaction between the surface and adsorbates. Sulfur could influence the surface properties, creating additional functional sites for adsorption and enhancing the overall adsorption capacity of the material. This difference in elemental composition between ZnO and gunningite suggests that gunningite may offer better performance in adsorption-based applications, particularly in photocatalytic processes, due to its higher zinc and sulfur content.

Sulfur vacancies in Gunningite can operate as active sites for charge carrier separation, increasing photocatalytic efficiency. The insertion of sulfur vacancies increases electron mobility while decreasing photogenerated charge carrier recombination rates [26]. The addition of sulfur can alter the electronic structure of Gunningite, resulting in a larger light absorption spectrum. This increase enables the material to use a broader range of the solar spectrum, which is advantageous for photocatalytic applications [27]. Gunningite's sulfur contributes to the charge carrier dynamics' optimization. Sulfur may lower electron and hole recombination rates and stabilize excited states, all of which are essential for sustaining strong photocatalytic activity [28].

Table 2. Element content of sample by EDX analysis

Sample	% Wt		
	Zn	O	S
Gunningite	77	21	2
Wurtzite	69	31	-

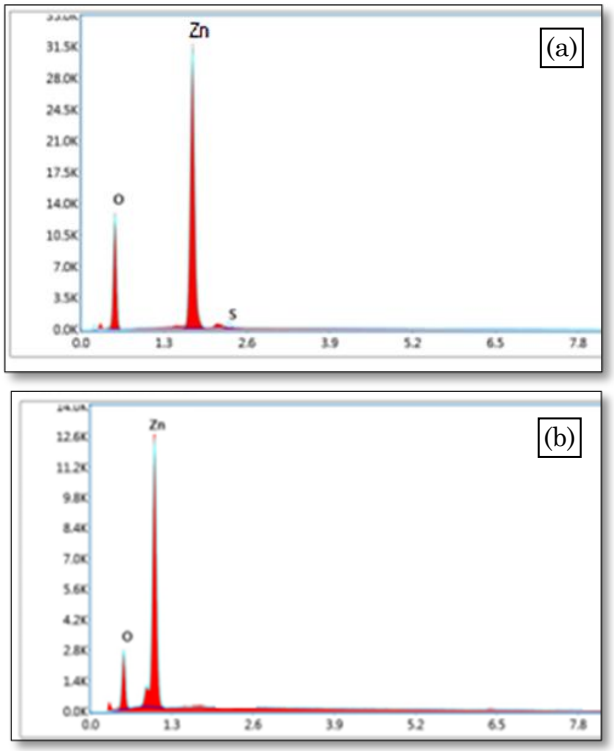

Figure 9. EDX for mapping analysis for (a) Gunningite ($ZnSO_4 \cdot H_2O$) and (b) Wurtzite (ZnO)

Sulfur species can interact with photogenerated holes, effectively trapping them and inhibiting recombination. This interaction increases the availability of reactive species for photocatalytic processes [26]. When coupled with other elements or compounds, sulfur can have synergistic effects that increase photocatalytic activity. Sulfur, for example, when combined with other materials to make metal sulfides or composites, can increase overall performance by optimizing electrical characteristics [29].

Table 3 highlights the role of different surfactants, including gelatin, in synthesizing various materials and their corresponding catalytic and physicochemical properties. Gelatin stands out as a natural surfactant with significant contributions to material synthesis, particularly in replacing synthetic surfactants. Unlike synthetic surfactants like CTAB, SDS, and SDBS, which are costly, have low sustainability, and involve complex production processes with hazardous chemicals, gelatin offers a more sustainable and economical alternative. Derived from abundant and inexpensive by-products such as animal bones or skin, gelatin provides an environmentally friendly and cost-effective solution for large-scale material production.

Several studies, including this work, demonstrate that gelatin significantly enhances the physicochemical and catalytic properties of materials. For example, in this research, gelatin-assisted synthesis improved the adsorption and photocatalytic performance of gunningite, achieving an efficiency of 87%. Similarly, gelatin as a co-template in iron oxide synthesis resulted in high photocatalytic performance, while its use in mesoporous silica enhanced adsorption capabilities. These results underscore gelatin's ability to produce materials with superior physicochemical properties and competitive catalytic performance compared to those synthesized with synthetic surfactants. For industrial applications, gelatin's abundance, low cost, and excellent performance make it a promising candidate for sustainable material synthesis.

Table 4 compares the band gap values and photocatalytic performance of various zinc-based materials for methylene blue (MB) photodegradation. It shows that the band gap of these materials varies, with ZnO nanostructures exhibiting a band gap of 3.35 eV, which is commonly associated with high photocatalytic activity for MB degradation. Materials, such as

Table 3. Comparison of material performance different typeof surfactan

Material	Surfactant Type	Synthesis Conditions	Physicochemical Properties	Catalytic Performance	Ref
Wurtzite ZnO	None	Combustion synthesis at 400°C	Hexagonal wurtzite structure with lattice constants a=3.2511 Å, c=5.2076 Å	Not reported	[30]
Wurtzite ZnO	None	Low-temperature synthesis	Fluorescent nanoparticles	Not reported	[31]
MoS_2	CTAB, SDS, SDBS	Hydrothermal synthesis with single precursors	Morphology varies depending on surfactant	HDS activity varies; MoS_2-SDBS exhibited superior performance	[32]
Hierarchical Mordenite	[3-(Trimethoxysilyl)propyl]octadecyldimethylammonium chloride (TPOAC)	Hydrothermal synthesis with TPOAC/SiO_2 molar ratio	Mesoporous structure with uniform distribution	High stability and selectivity in benzene alkylation	[33]
Nanoporous Gold	None	Dealloying through cyclic electrode potential	Surface-dominant {111} or {100}	Enhanced electrocatalytic activity	[34]
ZSM-5 Zeolite	Novel anionic surfactant	Hydrothermal synthesis	Hierarchical structure	Superior catalytic performance	[35]
Hydroxyapatite (HAP)	Various surfactants	Surfactant-assisted synthesis	Varies in morphology and chemical properties	Activity in CO oxidation	[36]
ZnO/Mesoporous Silica	Gelatin- P123	Bisurfactant -assisted synthesis	Mesoporous structure	Efficiency 92%	[37]
Polymeric Surfactants	None	Catalyzed condensation	Surface-active polymers	Potential for catalytic applications	[38]
Noble Metal Nanoparticles	None	Colloidal synthesis	Surfactant-free nanoparticles	Improved catalytic activity	[39]
Mesoporous silica	gelatin	gelatin as pore expander	Gelatin as natural surfactan	High adsorption performance	[40]
Iron oxide	Gelatin	Gelatin assited surfactant	Gelatin as co-template	High photocatalytic performance	[41]
Gunningite	gelatin	Gelatin assited surfactant	Gelatin as co-template	Efficiency 87%	This Work

ZnO doped with chloride ions display a band gap range of 2.99 to 2.59 eV, which corresponds to an increased MB degradation efficiency as chloride concentration rises. The reduction in band gap is typically linked to enhanced photocatalytic activity, allowing these materials to utilize a broader spectrum of light, including visible light, for the photodegradation process.

Although the band gap values for gunningite and wurtzite were not measured in this study, based on trends observed in similar materials, it can be predicted that their band gaps would fall within a range that facilitates efficient photodegradation of methylene blue to CO_2 and water. In particular, materials with lower band gaps, such as those in the ZnO doped with chloride range, typically exhibit improved photocatalytic performance under visible light, which is advantageous for large-scale applications. If this prediction is confirmed by experimental results, these materials, including gunningite and wurtzite, could offer effective and sustainable alternatives for the photodegradation of organic pollutants like methylene blue, aligning with the trends seen in other zinc-based photocatalysts.

Zinc-based photocatalysts exhibit significant potential for large-scale applications due to their outstanding reusability and stability in photodegradation processes. As shown in the Table 5, materials like ZnO nanorods maintain high efficiency over multiple cycles, with only a slight decline from 83% to 80% over four cycles, demonstrating exceptional durability. Similarly, Ag/ZnO nanocomposites and Ag-ZnO nanocatalysts exhibit notable recyclability, with minor efficiency losses even after several reuse cycles, making them highly promising for industrial applications. Their ability to retain more than 80% of their initial photodegradation efficiency highlights their resilience under repetitive use, a critical requirement for cost-effective, large-scale deployment.

Table 4. Band gap of zinc based material for methylene blue photodegradation

Sample Name	Band Gap (eV)	Photocatalytic Performance on Methylene Blue	Reference
ZnO Doped with Chloride Ions	2.99 – 2.59	Increased MB degradation efficiency with higher chloride concentration	[42]
Ag-Doped ZnO	Not mentioned	Enhanced photocatalytic activity under visible light	[43]
ZnO Nanostructures	3.35	High photocatalytic activity for MB degradation	[44]
ZnO Nanostructures with Chloride	3.42 – 3.16	Improved MB degradation efficiency with lower band gap	[30]

Table 5. Reusability and stability of catalyst based zinc materials for methylene blue photodegradation

Sample Name	Reusability	Stability	Note	Reference
ZnO Nanorods	83% (cycle 1), 83% (cycle 2), 81% (cycle 3), 80% (cycle 4)	Slight decrease in efficiency (less than 3% after 4 cycles)	Excellent reusability with minimal decline in efficiency after four cycles	[45]
Ag/ZnO Nanocomposite	Slight decrease after five cycles in removing MB, MO, CR dyes	Significant recyclability, slight efficiency loss after 5 cycles	Significant recyclability for organic dye removal	[46]
Ag-ZnO Nanocatalyst	95% (cycle 1), 89.5% (cycle 4)	High stability, slight reduction in photodegradation efficiency	High stability with minor reduction in efficiency after four cycles	[44]
ZnO NPs	93.25% (cycle 1), 86.63% (cycle 5) (MB), 91.06% (cycle 1), 83.61% (cycle 5) (Rhodamine B)	High stability with less than 10% reduction in efficiency after 5 cycles	Excellent photocatalytic activity with high stability after five cycles	[25]
Mg-ZnO Nanorods	82% (cycle 1), 75% (cycle 4)	Slight decrease in efficiency (from 82% to 75% after 4 cycles)	Slight reduction in efficiency after four cycles of photodegradation of MB and ciprofloxacin	[47]

Furthermore, the stability of zinc-based materials ensures consistent performance in degrading methylene blue and other organic pollutants. For instance, ZnO nanoparticles show less than a 10% reduction in efficiency after five cycles, indicating robust structural integrity and chemical resilience. The slight efficiency losses observed in Mg-ZnO nanorods and other zinc composites suggest that further optimization could yield even more durable catalysts. These attributes, combined with their scalability and compatibility with existing technologies, position zinc-based photocatalysts as key candidates for addressing environmental challenges in wastewater treatment and beyond. Their promise in large-scale applications lies in their capacity to combine efficiency, stability, and reusability, making them an ideal solution for sustainable photocatalysis.

Although gunningite and wurtzite were not specifically tested for reusability and stability in this study, observing the trends in the table suggests that these materials may exhibit similar properties. Zinc-based photocatalysts, as demonstrated by ZnO nanorods, Ag/ZnO nanocomposites, and other derivatives, generally show high reusability and stability with minimal efficiency loss over multiple cycles. This trend highlights the robustness of zinc-based materials, which retain their structural integrity and photocatalytic activity even after prolonged use.

Considering their chemical composition and similarity to other zinc-based catalysts, it is reasonable to predict that gunningite and wurtzite could exhibit excellent reusability and stability in photodegradation applications. These materials are likely to maintain a high percentage of their initial efficiency over several cycles, with only slight reductions, aligning with the performance trends observed for other zinc-based photocatalysts. This prediction further emphasizes the potential of gunningite and wurtzite as promising candidates for sustainable and large-scale photocatalytic applications in the future.

Table 6 and Figure 10 presents data on the photodegradation kinetics of methylene blue on two materials, gunningite and wurtzite, analyzed using three kinetic models: pseudo-zero-order, pseudo-first-order, and pseudo-second-order. Based on the coefficient of determination (R^2), the pseudo-first-order model provides the best fit for both materials, with R^2 values of 0.9979 for gunningite and 0.9938 for wurtzite. These high R^2 values suggest that the photodegradation kinetics are predominantly governed by the pseudo-first-order mechanism, implying that the degradation rate is directly proportional to the methylene blue concentration.

Furthermore, the reaction rate constants (k) for the pseudo-first-order model reveal differences in the photodegradation efficiency of the two materials. Gunningite exhibits a k value of 0.0226, which is higher than that of wurtzite at 0.014, indicating that gunningite is more effective at degrading methylene blue under the studied conditions. In contrast, the pseudo-zero-order and pseudo-second-order models yield lower R^2 values, indicating their limited suitability in describing the photodegradation kinetics compared to the pseudo-first-order model. These findings underscore the relevance of the pseudo-first-order

Table 6. Kinetic of methylene blue photodegradation of gunningite and wurztite

Sample	C_O (ppm)	Model					
		Pseudo Zero Order		Pseudo first order		Pseudo second order	
		k	R^2	K	R^2	k	R^2
Gunningite	5	0.00449	0.9164	0.0226	0.9979	0.0146	0.9247
Wurtzite	5	0.03750	0.9483	0.014	0.9938	0.0058	0.9719

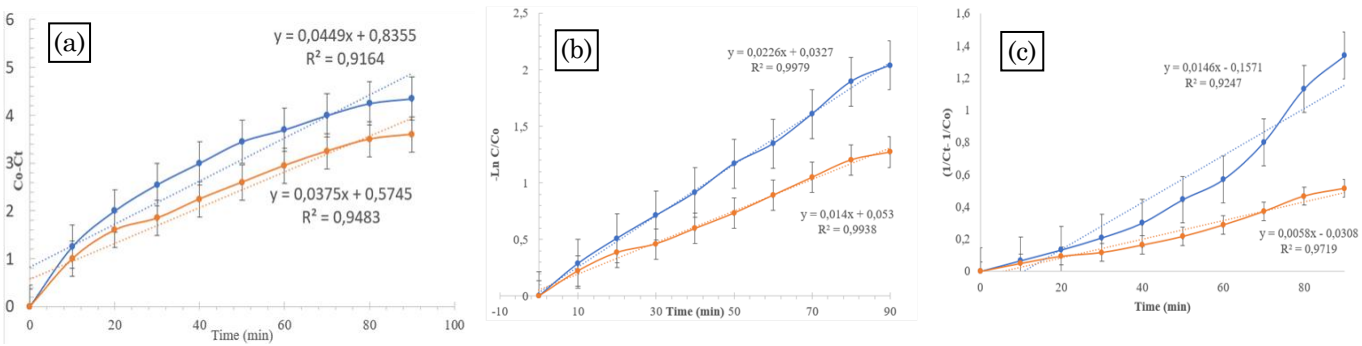

Figure 10. Kinetic of Guninggite (blue line) and Wurtzite (orange line) use model Pseudo- (a) Zero; (b) First; and (c) Second order plot of methylene blue photodegradation

model in characterizing the photocatalytic degradation behavior of methylene blue on both materials.

4. Conclusion

In conclusion, this study emphasizes the significant potential of Gunningite ($ZnSO_4 \cdot H_2O$) and Wurtzite (ZnO) nanoparticles, synthesized using gelatin-based colloids, for advanced photocatalytic applications. Gunningite demonstrated exceptional photocatalytic performance, achieving 87% degradation of methylene blue under UV light, compared to 72% for Wurtzite. The enhanced activity of Gunningite is attributed to its higher specific surface area of 61.5 m^2/g, in contrast to Wurtzite's 11.4 m^2/g, which provides more active sites for adsorption and facilitates faster interaction with the dye. X-ray diffraction (XRD) analysis confirmed the successful formation of both materials, with Gunningite showing characteristic peaks corresponding to $ZnSO_4 \cdot H_2O$, while Wurtzite displayed typical ZnO patterns. Fourier Transform Infrared (FTIR) spectroscopy indicated distinct functional groups in both materials, with Gunningite showing additional sulfur-related peaks (S–O and O=S=O), which were absent in Wurtzite, confirming the presence of sulfur. Elemental analysis via Energy Dispersive X-ray (EDX) revealed that Gunningite contained 71% zinc, 21% oxygen, and 2% sulfur, while Wurtzite consisted of 69% zinc and 31% oxygen, reflecting the differences in their composition and highlighting the impact of sulfur on Gunningite's enhanced performance.

These findings underscore the critical role of surface properties, composition, and tailored synthesis in the development of more efficient photocatalysts. With its high photocatalytic efficiency, larger surface area, and unique sulfur content, Gunningite offers significant promise for environmentally sustainable solutions in the degradation of organic pollutants, particularly in wastewater treatment. Further studies could explore the scalability of this synthesis method and its industrial applicability for large-scale environmental remediation.

Acknowledgements

We would like to express our heartfelt gratitude to Universitas Sebelas Maret, Indonesia, for their invaluable support in providing funding for the Research by International Research Collaboration 2025.

CRediT Author Statement Author

Author Contributions: M. Ulfa: Conceptualization, Investigation, Resources, Data Curation, Writing, Review and Editing, Supervision; M. Ulfa and H. Aziza Methodology, Formal Analysis, Data Curation, Writing Draft Preparation; M. Ulfa and H. Aziza : Review and Editing, Data Curation, and Validation. All authors have read and agreed to the published version of the manuscript

References

[1] Ducher, M., Blanchard, M., Balan, E. (2018). Equilibrium isotopic fractionation between aqueous Zn and minerals from first-principles calculations. *Chem. Geol.* 483, 342–350. DOI: 10.1016/j.chemgeo.2018.02.040

[2] Babikier, M., Wang, D., Wang, J., Li, Q., Sun, J., Yan, Y., Yu, Q., Jiao, S. (2014). Fabrication and properties of sulfur (S)-doped ZnO nanorods. *Journal of Materials Science: Materials in Electronics*, 25 (1), 157–162. DOI: 10.1007/s10854-013-1566-7.

[3] Ulfa, M., Iswanti, Y., Irwanti, Y., Sholeha, N.A., Masruchin, N., Subagyo, R., Bahruji, H., Prasetyoko, D. (2023). Hydrothermal effect of gunningite use Pluronic F127-Gelatin as template and the ibuprofen adsorption performance. *Heliyon*, 9 (3), e14473. DOI: 10.1016/j.heliyon.2023.e14473.

[4] Lhimr, S., Bouhlassa, S., Ammary, B. (2019). Effect of molar ratio on structural and size of ZnO/C Nanocomposite Synthesized Using a colloidal method at low temperature. *Indonesian Journal of Chemistry*, 19(2), 422–429. DOI: 10.22146/ijc.37932.

[5] Prasetyoko, D., Sholeha, N.A., Subagyo, R., Ulfa, M., Bahruji, H., Holilah, H., Pradipta, M.F., Jalil, A.A. (2023). Mesoporous ZnO nanoparticles using gelatin — Pluronic F127 as a double colloidal system for methylene blue photodegradation. *Korean Journal of Chemical Engineering*, 40(1), 112–123. DOI: 10.1007/s11814-022-1224-y.

[6] Shin, J., Andreas Hutomo, C., Kim, J., Jang, J., Beum Park, C. (2022). Natural pollen exine-templated synthesis of photocatalytic metal oxides with high surface area and oxygen vacancies. *Applied Surface Science*, 599(June), 154064. DOI: 10.1016/j.apsusc.2022.154064.

[7] Ulfa, M., Ari, M., Ali, P. (2022). Influence of Calcination Temperatures on Gunningite-Based Gelatin Template and Its Application as Ibuprofen Adsorption. 22(6), 1–9. DOI: 10.22146/ijc.77004.

[8] Lyu, Y., Sun, Z., Xin, Y., Liu, Y., Wang, C., Liu, X. (2019). Reactivation of spent S-Zorb adsorbents for gasoline desulfurization. *Chemical Engineering Journal*, 374(May), 1109–1117. DOI: 10.1016/j.cej.2019.06.010.

[9] Rondius, B. (2012). Vibrational spectroscopic study of the zinc sulfate minerals gunningite and namuwite. *Journal of Molecular Structure*, 1023, 1–11. DOI: 10.1016/j.molstruc.2012.04.056.

[10] Li, J., Han, L., Zhang, T., Qu, C., Yu, T., Yang, B. (2022). Removal of Methylene Blue by Metal Oxides Supported by Oily Sludge Pyrolysis Residues. *Applied Sciences (Switzerland)*, 12(9) DOI: 10.3390/app12094725.

[11] Idris, N.J., Bakar, S.A., Mohamed, A., Muqoyyanah, M., Othman, M.H.D., Mamat, M.H., Ahmad, M.K., Birowosuto, M.D., Soga, T. (2021). Photocatalytic performance improvement by utilizing GO_MWCNTs hybrid solution on sand/ZnO/TiO2-based photocatalysts to degrade methylene blue dye. *Environmental Science and Pollution Research*, 28(6), 6966–6979. DOI: 10.1007/s11356-020-10904-y.

[12] Albiss, B., Abu-Dalo, M. (2021). Photocatalytic degradation of methylene blue using zinc oxide nanorods grown on activated carbon fibers. *Sustainability (Switzerland)*, 13(9) DOI: 10.3390/su13094729.

[13] Saramas, D., Ekgasit, S. (2021). Nano-zinc oxide-doped activated carbon from popped rice and its application for feed additive. *Engineering Journal*, 25(3), 41–50. DOI: 10.4186/ej.2021.25.3.41.

[14] Lihitkar, P.B., Violet, S., Shirolkar, M., Singh, J., Srivastava, O.N., Naik, R.H., Kulkarni, S.K. (2012). Confinement of zinc oxide nanoparticles in ordered mesoporous silica MCM-41. *Materials Chemistry and Physics*, 133(2–3), 850–856. DOI: 10.1016/j.matchemphys.2012.01.106.

[15] Wu, M., Shi, L., Lim, T.T., Veksha, A., Yu, F., Fan, H., Mi, J. (2018). Ordered mesoporous Zn-based supported sorbent synthesized by a new method for high-efficiency desulfurization of hot coal gas. *Chemical Engineering Journal*, 353 (July), 273–287. DOI: 10.1016/j.cej.2018.07.134.

[16] Venkatesan, S., Suresh, S., Ramu, P., Kandasamy, M., Arumugam, J., Thambidurai, S., Prabu, K.M., Pugazhenthiran, N. (2022). Biosynthesis of zinc oxide nanoparticles using Euphorbia milii leaf constituents: Characterization and improved photocatalytic degradation of methylene blue dye under natural sunlight. *Journal of the Indian Chemical Society*, 99(5), 100436. DOI: 10.1016/j.jics.2022.100436.

[17] Ulfa, M., Nisa, D., Muhammad, F.P., Prasetyoko, D. (2021). Investigating the Hydrophilicity of Zinc Oxide Nanoparticles Using Xylene and Water for Ibuprofen Adsorption. *Journal of Chemical Technology and Metallurgy*, 56(4), 761–768.

[18] Zerdali, M., Hamzaoui, S., Teherani, F.H., Rogers, D. (2006). Growth of ZnO thin film on SiO2/Si substrate by pulsed laser deposition and study of their physical properties. *Materials Letters*, 60(4), 504–508. DOI: 10.1016/j.matlet.2005.09.024.

[19] Ivanova, T., Harizanova, A., Koutzarova, T., Vertruyen, B., Closset, R. (2024). Sol–Gel Synthesis of ZnO:Li Thin Films: Impact of Annealing on Structural and Optical Properties. *Crystals*, 14(1). DOI: 10.3390/cryst14010006.

[20] Seki, T., Chiang, K.Y., Yu, C.C., Yu, X., Okuno, M., Hunger, J., Nagata, Y., Bonn, M. (2020). The bending mode of water: A powerful probe for hydrogen bond structure of aqueous systems. *Journal of Physical Chemistry Letters*, 11(19), 8459–8469. DOI: 10.1021/acs.jpclett.0c01259.

[21] Fatoni, A., Hasanah, M., Sirumapea, L., Putri, A.D., Sari, K., Khairani, R.D., Hidayati, N. (2023). Synthesis, Characterization of Polyvinyl Alcohol-Chitosan-ZnO/CuO Nanoparticles Film and Its Biological Evaluation as An Antibacterial Agent of Staphylococcus aureus. *al-Kimiya*, 10(1), 1–12. DOI: 10.15575/ak.v10i1.24725.

[22] Hassen, A., Moawed, E.A., Bahy, R., El Basaty, A.B., El-Sayed, S., Ali, A.I., Tayel, A. (2024). Synergistic effects of thermally reduced graphene oxide/zinc oxide composite material on microbial infection for wound healing applications. *Scientific Reports*, 14(1), 22942. DOI: 10.1038/s41598-024-73007-5.

[23] Motakef Kazemi, N., Asadi, A. (2022). Methylene Blue Adsorption from Aqueous Solution Using Zn2(Bdc)2(Dabco) Metal-Organic Framework and Its Polyurethane Nanocomposite. *Iranian Journal of Chemistry and Chemical Engineering*, 41(12), 4026–4038. DOI: 10.30492/IJCCE.2022.538689.4926.

[24] Hosseini, S., Mashaykhi, S., Babaei, S., Afr, S. (2016). Preparation of Graphene Oxide (GO). *J Chem*, 69, 105–112. DOI: 10.17159/0379-4350/2016/v69a13

[25] Ahmadi, S., Igwegbe, C.A. (2020). Removal of Methylene Blue on Zinc Oxide Nanoparticles: Nonlinear and Linear Adsorption Isotherms and Kinetics Study. *Sigma Journal of Engineering and Natural Sciences*, 38(1), 289–303. DOI: 10.3390/w14111749

[26] Ren, Z., Li, Y., Ren, Q., Zhang, X., Fan, X., Liu, X., Fan, J., Shen, S., Tang, Z., Xue, Y. (2024). Unveiling the Role of Sulfur Vacancies in Enhanced Photocatalytic Activity of Hybrids Photocatalysts. *Nanomaterials*, 14(12). DOI: 10.3390/nano14121009.

[27] Tateishi, I., Furukawa, M., Katsumata, H., Kaneco, S. (2024). Effective Utilization of Sulfur Wastewater by Photocatalytic System Using B/CuO/ZnO. *Separations*, 11(1). DOI: 10.3390/separations11010019.

[28] Murugan, S., Ashokkumar, M., Sakthivel, P., Choi, D. (2023). Sulfur deficiency mediated visible emission of ZnS QDs by magnesium dopant and their application in waste water treatment. *Heliyon*, 9(7), e17947. DOI: 10.1016/j.heliyon.2023.e17947.

[29] Qi, Z., Chen, J., Zhou, W., Li, Y., Li, X., Zhang, S., Fan, J., Lv, K. (2023). Synergistic effects of holey nanosheet and sulfur-doping on the photocatalytic activity of carbon nitride towards NO removal. *Chemosphere*, 316, (October 2022), 137813. DOI: 10.1016/j.chemosphere.2023.137813.

[30] Reddy, A.J., Kokila, M.K., Nagabhushana, H., Rao, J.L., Shivakumara, C., Nagabhushana, B.M., Chakradhar, R.P.S. (2011). Combustion synthesis, characterization and Raman studies of ZnO nanopowders. *Spectrochimica Acta - Part A: Molecular and Biomolecular Spectroscopy*, 81(1), 53–58. DOI: 10.1016/j.saa.2011.05.043.

[31] Khan, Y., Durrani, S.K., Mehmood, M., Ahmad, J., Khan, M.R., Firdous, S. (2010). Low temperature synthesis of fluorescent ZnO nanoparticles. *Applied Surface Science*, 257(5), 1756–1761. DOI: 10.1016/j.apsusc.2010.09.011.

[32] Chu, S., Zhou, W., Zhang, C., Zheng, Y., Liu, Y., Liu, Y. (2020). Relationship between the structure and catalytic performance of MoS2 with different surfactant-assisted syntheses in the hydrodesulfurization reaction of 4,6-DMDBT. *RSC Advances*, 10(13), 7600–7608. DOI: 10.1039/c9ra08407j.

[33] Liu, M.N., Li, Y.Z., Xie, Z.X., Hao, Q.Q., Luo, Q.X., Zhang, J., Chen, H., Dai, C., Ma, X. (2020). Organosilane surfactant-directed synthesis of hierarchical mordenite with enhanced catalytic performance in the alkylation of benzene with 1-dodecene. *New J. Chem*. 44:16638–16644. DOI: 10.1039/D0NJ03420A

[34] Zhili, W., Pan, L., Jiuhui, H., Chun, C., Shoucong, N., Akihiko, H., Takeshi, F., Mingwei, C. (2017). Engineering the internal surfaces of three-dimensional nanoporous catalysts by surfactant-modified dealloying. *Natural Communication*, 10(3), 33–43. DOI: 10.1038/s41467-017-01085-3

[35] Sabarish, R., Unnikrishnan, G. (2020). A novel anionic surfactant as template for the development of hierarchical ZSM-5 zeolite and its catalytic performance. *Journal of Porous Materials*, 27(3), 691–700. DOI: 10.1007/s10934-019-00852-5.

[36] Hajimirzaee, S., Chansai, S., Hardacre, C., Banks, C.E., Doyle, A.M. (2019). Effects of surfactant on morphology, chemical properties and catalytic activity of hydroxyapatite. *Journal of Solid State Chemistry*, 276, 345–351. DOI: 10.1016/j.jssc.2019.05.031.

[37] Ulfa, M., Nur, C., Amalia, N. (2023). Fine-tuning mesoporous silica properties by a dual-template ratio as TiO2 support for dye photodegradation booster. *Heliyon*, 9(6), e16275. DOI: 10.1016/j.heliyon.2023.e16275.

[38] Goddard, A.R., Apebende, E.A., Lentz, J.C., Carmichael, K., Taresco, V., Irvine, D.J., Howdle, S.M. (2021). Synthesis of water-soluble surfactants using catalysed condensation polymerisation in green reaction media. *Polymer Chemistry*, 12 (20), 2992–3003. DOI: 10.1039/d1py00415h.

[39] Quinson, J., Kunz, S., Arenz, M. (2023). Surfactant-Free Colloidal Syntheses of Precious Metal Nanoparticles for Improved Catalysts. *ACS Catalysis*, 13(7), 4903–4937. DOI: 10.1021/acscatal.2c05998.

[40] Ulfa, M., Prasetyoko, D., Trisunaryanti, W., Bahruji, H., Fadila, Z.A., Sholeha, N.A. (2022). The effect of gelatin as pore expander in green synthesis mesoporous silica for methylene blue adsorption. *Scientific Reports*, 12(1), 1–12. DOI: 10.1038/s41598-022-19615-5.

[41] Ulfa, M., Prasetyoko, D., Bahruji, H. (2021). Hexagonal Flake- Like Hematite (α -Fe 2 O 3) Prepared by Hybrid Pluronic F127-Gelatin as Eco-Friendly Template for Adsorption of Ibuprofen. 1–15. DOI: 10.3390/ma14226779

[42] Alshgari, R.A., Ujjan, Z.A., Shah, A.A., Bhatti, M.A., Tahira, A., Shaikh, N.M., Kumar, S., Ibupoto, M.H., Elhawary, A., Nafady, A., Vigolo, B., Ibhupoto, Z.H. (2022). ZnO Nanostructures Doped with Various Chloride Ion Concentrations for Efficient Photocatalytic Degradation of Methylene Blue in Alkaline and Acidic Media. *Molecules*, 27(24) DOI: 10.3390/molecules27248726.

[43] Saad, A.M., Abukhadra, M.R., Abdel-Kader Ahmed, S., Elzanaty, A.M., Mady, A.H., Betiha, M.A., Shim, J.J., Rabie, A.M. (2020). Photocatalytic degradation of malachite green dye using chitosan supported ZnO and Ce–ZnO nano-flowers under visible light. *Journal of Environmental Management*, 258, 110043. DOI: 10.1016/j.jenvman.2019.110043.

[44] Akyüz, D. (2021). rGO-TiO2-CdO-ZnO-Ag photocatalyst for enhancing photocatalytic degradation of methylene blue. *Optical Materials*, 116, (January), 111090. DOI: 10.1016/j.optmat.2021.111090.

[45] Davis, K., Yarbrough, R., Froeschle, M., White, J., Rathnayake, H. (2019). Band gap engineered zinc oxide nanostructures: Via a sol-gel synthesis of solvent driven shape-controlled crystal growth. *RSC Advances*, 9(26), 14638–14648. DOI: 10.1039/c9ra02091h.

[46] Negash, A., Mohammed, S., Weldekirstos, H.D., Ambaye, A.D., Gashu, M. (2023). Enhanced Photocatalytic Degradation of Methylene Blue Dye Using Eco-Friendly Synthesized rGO-ZnO Nanocomposites. *Scientific Reports*, 13(1), 22234. DOI: 10.1038/s41598-023-48826-7.

[47] Ikram, M., Aslam, S., Haider, A., Naz, S., Ul-Hamid, A., Shahzadi, A., Ikram, M., Haider, J., Ahmad, S.O.A., Butt, A.R. (2021). Doping of Mg on ZnO Nanorods Demonstrated Improved Photocatalytic Degradation and Antimicrobial Potential with Molecular Docking Analysis. *Nanoscale Research Letters*, 16(1). DOI: 10.1186/s11671-021-03537-8.